

Adaptive Bayesian Beamforming for Imaging by Marginalizing the Speed of Sound

Kyurae Kim, *Member, IEEE*, Simon Maskell, *Member, IEEE*, and Jason F. Ralph

arXiv:2212.03824v3 [eess.SP] 15 Sep 2025

Abstract—Imaging methods based on array signal processing often require a fixed propagation speed of the medium, also known as the speed of sound (SoS) for methods based on acoustic signals. The resolution of the images formed using these methods is strongly affected by the assumed SoS, which, due to multipath, nonlinear propagation, and non-uniform mediums, is challenging to select. In this correspondence, we propose a Bayesian approach to marginalize the influence of the SoS on beamformers for imaging. In particular, we adapt a previously proposed Bayesian direction-of-arrival estimation model to the imaging setting, where we model the uncertainty of the SoS and then compute the posterior expectation of the popular minimum variance distortionless response beamformer (MVDR), resulting in a method we call *Bayes MVDR*. Furthermore, we demonstrate that the marginal likelihood (ML) of the model can be used for imaging. To solve the Bayesian integral efficiently, we use numerical Gauss-Hermite quadrature and apply our proposed approach to shallow water sonar imaging where multipath and nonlinear propagation are abundant. We compare Bayes MVDR and ML with the standard MVDR beamformer and demonstrate that its Bayesian counterpart achieves improved range and azimuthal resolution while effectively suppressing multipath artifacts.

Index Terms—Bayesian methods, adaptive beamforming, sonar imaging, array signal processing.

I. INTRODUCTION

BEAMFORMING algorithms [1, 2, 3] for imaging require accurate physical modeling of the system to achieve high resolution. It is often assumed that the signal propagates in a linear “direct path” with a globally fixed propagation speed of the medium. This model is “wrong but useful”, as George Box would comment, but discrepancies between the actual physics and the model result in lower image resolution and artifacts [4]. For example, sonar imaging in shallow waters suffers from multipath artifacts [5], ultrasound imaging has to deal with inhomogeneous media [6, 7]. Since we focus on applications with complex acoustic propagation (such as sonar, medical ultrasound, and seismology), with some loss of generality, we will hereafter refer to the propagation speed as the speed of sound (SoS).

Modeling the SoS of sonar is particularly difficult since the propagation speed varies by depth, salinity, ocean temperature, and weather. As such, modeling the SoS profile [8, §9.1.2] is challenging, and the resulting profile will often be imperfect. As such, for beamforming, selecting the right SoS is not only

K. Kim is with the University of Pennsylvania, Philadelphia, United States (e-mail: kyrkim@seas.upenn.edu).

S. Maskell and J. F. Ralph are with the University of Liverpool, Liverpool, United Kingdom (e-mail: {S.Maskell, jfralph}@liverpool.ac.uk).

difficult, but any fixed choice will often suffer from modeling imperfections.

Various approaches have been proposed to combat the issue of SoS selection. Some authors have proposed to statistically estimate the propagation speed [9, 10], and some of these have been specifically proposed in the context of beamforming [7]. Although the method of Stahli *et al.* [9] provides pixel-wise estimates of the SoS, it requires *a priori* segmentation of the target field, and its utility for beamforming has yet to be studied.

Meanwhile, adaptive beamformers, such as variants of the minimum-variance distortionless response (MVDR) beamformer, which are purely statistical signal processing-based approaches, [2, 11] have been shown to be effective against SoS mismatch [4] and other inconveniences such as cross-channel interference, noise [12], and multipath [5]. However, these approaches do not directly try to *correct* the chosen SoS. In this work, we extend MVDR in a way that directly deals with the imperfections in the choice of SoS by modeling it as an uncertain quantity via probabilistic modeling. In particular, our probabilistic model is inspired by the approach of Bell *et al.* [13]. By estimating the uncertainty of the SoS, we are able to *marginalize* it, resulting in a marginalized beamformer achieving better resolution.

Bell *et al.* [13] proposed what they call the Bayesian robust adaptive (BRA) for direction-of-arrival (DoA) estimation. In more detail, they adapt MVDR by performing Bayesian inference of the optimal beam steering direction, where the likelihood uses the covariance of the received signal. The posterior can be used to marginalize the steering direction used within the MVDR beamformer [14]. The Bayesian robust adaptive (BRA) beamformer has been further extended for multiple DoA estimation [15] and passive sonar detection [16], while the convergence of this method has been established by Lam and Singer [17].

When applying beamforming to imaging, each pixel in the image becomes a focal point. Therefore, the DoA estimation framework of [13] cannot be applied directly. However, in this correspondence, we demonstrate that the DoA estimation framework can be used for pixel-wise SoS estimation. Firstly, we estimate the pixel-wise SoS by adopting the likelihood of the BRA beamformer. Then, the SoS used to compute the MVDR beamformer is marginalized over the posterior for the SoS forming what we call “*Bayes MVDR*.” Our approach provides a data-driven way to handle uncertainties associated with the propagation model by expressing them as uncertainties in the SoS. Furthermore, by adopting a probabilistic model for the acquired signals, we can now compute the

evidence, or marginal likelihood, which can be used to detect the presence of signals in contrast to noise. We demonstrate that this quantity, denoted “ML” in the experiments, can be used for imaging and can further suppress noise and multipath artifacts compared to Bayes MVDR. For posterior inference, we employ Gauss-Hermite quadrature, which, unlike previous works in Bayesian DoA estimation, enables the proper use of priors with continuous support, such as Gaussians.

We evaluate our method by applying it to active sonar imaging. We use the Bellhop propagation model [18, 19] to simulate point targets. Compared to the MVDR beamformer [12, 14, 20, 21] popularly used in sonar imaging [22, 23, 24, 25, 26, 27, 28], our method effectively suppresses multipath artifacts while achieving lower sidelobes and improved azimuth resolution.

To summarize, our contributions are as follows:

- We propose a Bayesian model for estimating the speed of sound from the received signal on a pixel-by-pixel basis.
- We propose adaptive beamforming algorithms for imaging, Bayes MVDR and ML, which utilize the posterior of the SoS.
- We propose the use of an efficient numerical quadrature scheme for computing the posterior.

We discuss our motivations and the setup in more detail in Section II-II-A, where the signal model is described in Section II-II-B. The probabilistic model is presented in Section II-II-C, with the inference strategy in Section II-II-D and the resulting beamformer in Section II-II-E. We then present experimental results in Section III before concluding in Section IV.

II. ADAPTIVE BAYESIAN BEAMFORMING BY MARGINALIZING OF THE SPEED OF SOUND

A. Background and Motivation

Conventional Beamforming. The conventional delay-and-sum (DAS, [3]) beamforming method, also known as backprojection, is described as

$$y(p) = \sum_{n=1}^N w_n x_n(t(p, c, n)) = \mathbf{w}^\dagger \mathbf{x}^d(p, c), \quad (1)$$

where \dagger is the conjugate transpose, $x_n(t)$ is the signal sample received by the n th sensor at time t , p is the focal point (or image pixel), $y(p)$ is the beamformed response of p , c is the signal propagation speed of the medium, $n = 1, \dots, N$ is the sensor index, $t(p, c, n)$ is the round-trip time for the response of p to reach the n th sensor, w_n is known as the fading weight or apodization weight, \mathbf{w} is the fading weight vector, and $\mathbf{x}^d(p, c)$ is the delayed signals in vector form. The fading weights are often chosen independently of the received data to be off-the-shelf window functions, such as the Hann or Hamming windows.

The round-trip time $t(p, c, n)$ is computed as

$$t(p, c, n) = \frac{r(p, c, n)}{c} = \frac{r_{\text{TX}}(p, c) + r_{\text{RX}}(p, c, n)}{c}, \quad (2)$$

where $r(p, c, n)$ is the round-trip distance from the source to the n th array sensor, r_{TX} is the distance from source to the p , r_{RX} is the distance from p to the array sensor. In this work,

we consider a 2-dimensional imaging setting over the azimuth (x -axis) and range (y -axis).

Adaptive Beamforming. While simple and effective, DAS tends to result in poor resolution and high sidelobes. As a remedy, it is possible to *adapt* the fading weight to the received data, a scheme often called *adaptive* beamforming [2]. The most widely used approach is the celebrated minimum-variance distortionless response (MVDR) beamformer [14], also known as the Capon beamformer [29], which sets the fading weights as

$$\mathbf{w}(p, c) = \frac{\widehat{\Sigma}^{-1}(p, c) \mathbf{1}}{\mathbf{1}^\top \widehat{\Sigma}^{-1}(p, c) \mathbf{1}}, \quad (3)$$

where $\mathbf{1} = [1 \dots 1]^\top$ is a vector of ones, $\widehat{\Sigma}$ is the noise covariance of the signal at the focal point p given c , which is estimated from the received data. MVDR is known to greatly improve the resolution of the DAS beamformer while suppressing the sidelobes, provided that c has been set appropriately.

Choosing the Speed of Sound. Eq. (2) assumes that the signal propagates linearly and at a constant speed c , the SoS. Choosing c is crucial to the resolution of the resulting image for both conventional [7] and adaptive beamformers [4]. We assert that the common practice of choosing a globally fixed SoS is suboptimal. This is especially apparent in sonar applications where the propagation path is nonlinear and varies depending on oceanic parameters such as the SoS profile [8]. Furthermore, active sonar suffers from *multipath* [30], where a signal traveling between two points can take multiple paths of different lengths. Under the direct-path model with a single fixed SoS, multipath results in artifacts where the same target appears in multiple locations. In this work, we avoid this problem by incorporating the *uncertainty* of the SoS, which filters out these multipath artifacts.

B. Signal Model

Before presenting our Bayesian beamforming approach, we discuss our signal model. Let a signal be generated from a focal point p . The spectrum of this signal received by an N -sensor array is modeled as

$$\mathbf{x}(\omega) = s(p, \omega) \mathbf{a}(p, c) + \mathbf{n}(p, \omega) \quad (4)$$

where ω is the frequency, s is the envelope of the original target response, $\mathbf{a} \in \mathbb{C}^N$ is the steering vector defined as

$$\mathbf{a}(p, c) = [e^{j\omega t(p, c, 1)} \dots e^{j\omega t(p, c, N)}]^\dagger \quad (5)$$

for the time delay $t(p, c, n)$, j is the imaginary number, and $\mathbf{n} \in \mathbb{C}^N$ is the multivariate interference and noise vector. The dependence on c signifies that the response of the same focal point p can take different paths, which are identified by c .

The covariance of the received signal $\Sigma_{\mathbf{x}} \in \mathbb{C}^{N \times N}$ is

$$\Sigma_{\mathbf{x}}(p, c) = \sigma_s^2(p) \mathbf{a}(p, c) \mathbf{a}^\dagger(p, c) + \Sigma_{\mathbf{n}}(p), \quad (6)$$

where $\Sigma_{\mathbf{n}} \in \mathbb{C}^{N \times N}$ is the noise (and interference) covariance matrix. Note that if the data x_n is pre-delayed in the time domain by $t(p, c, n)$, the steering vector is replaced by a vector of 1s.

C. Probabilistic Model

Likelihood. We now describe our probabilistic model used to infer the SoS. Our likelihood is similar to that used by the BRA beamformer [13] and is described as

$$\ell_p(\mathbf{x}_{1:K} | c) = \prod_{l=1}^K \mathcal{CN}(\mathbf{x}_k(p, c); \mathbf{0}, \Sigma_{\mathbf{x}}(c, p)) \quad (7)$$

$$\propto |\Sigma_{\mathbf{x}}(p, c)|^{-K} \exp \left(-\sum_{l=1}^K \mathbf{x}_k^\dagger(p, c) \Sigma_{\mathbf{x}}^{-1}(p, c) \mathbf{x}_k(p, c) \right), \quad (8)$$

where \mathcal{CN} is the probability density function of a complex Gaussian and the data points $\mathbf{x}_k(p, c) \in \mathbb{C}^L$ are obtained by dividing the N sensor array into $K = N - L + 1$ overlapping subarrays such that $\mathbf{x}_k(p, c) = [x_{k+1} \ x_{k+2} \ \dots \ x_{k+L-1}]^\top$. Note that we have omitted the argument $t(p, c, l)$ for clarity. By using the subarray scheme [12], we avoid cancellation between coherent signals and obtain multiple samples without considering a temporal window. It also guarantees that the estimated covariance matrix is full-rank under mild assumptions [12].

The determinant in Eq. (8) penalizes covariances with large determinants, which implies that the signal is incoherent and has high variance, while the exponential term penalizes covariances that fail to explain the obtained data. Therefore, this likelihood selects values of c that, after focusing on the point p , gives rise to resulting observations that are coherent and low variance. Since the exact expression for $\Sigma_{\mathbf{x}}$ is unknown due to our lack of knowledge on $\Sigma_{\mathbf{n}}$ and σ_s^2 , approximation is required.

Approximate Likelihood. From the definition of $\Sigma_{\mathbf{x}}$ in Eq. (6), Bell *et al.* [13] have shown that the likelihood can be represented as

$$\ell_p(\mathbf{x}_{1:K} | c) \propto (1 + \sigma^2 \beta(c))^{-K} \times \exp \left(\frac{K \sigma_s^2 \beta^2(c) \mathbf{a}^\top \Sigma_{\mathbf{n}}^{-1}(c) \hat{\Sigma}_{\mathbf{n}}^{-1}(c) \Sigma_{\mathbf{n}}^{-1}(c) \mathbf{a}}{1 + \sigma^2 \beta(c)} \right) \quad (9)$$

where $\beta(c) = \mathbf{a}^\dagger \Sigma_{\mathbf{n}} \mathbf{a}$. Note that we have dropped the parameter p for clarity. To avoid dealing with $\Sigma_{\mathbf{n}}$, Bell *et al.* propose to further approximate the likelihood as

$$\ell_p(\mathbf{x}_{1:K} | c) \approx \tilde{\ell}_p(\mathbf{x}_{1:K} | c) = C \exp(K \gamma P_s(c)), \quad (10)$$

where $C > 0$ is some constant, P_s is the spectral estimate of the optimal output power σ_s^2 , and γ is a constant controlling the strength of the likelihood depending on the signal-to-noise (SNR) ratio.

The Capon [29] spectral estimate of the optimal output power is defined as

$$P_s(c) = (\mathbf{a}^\dagger \Sigma_{\mathbf{n}}^{-1}(c) \mathbf{a})^{-1} \quad (11)$$

and is the only point where the data enters our likelihood. Therefore, accurately estimating P_s is crucial to the performance of our beamformer. We further discuss this in Section II-II-D. Since $\Sigma_{\mathbf{n}}(c)$ is a nonlinear function of c , our model is not linear.

The power strength constant is defined as

$$\gamma = \frac{K}{\sigma_n^4} \frac{K \sigma_s^2 / \sigma_n^2}{1 + K \sigma_s^2 / \sigma_n^2} = \frac{K}{\text{NL}^2} \frac{K \text{SNR}}{1 + K \text{SNR}}, \quad (12)$$

where $\text{SNR} = \sigma_s^2 / \sigma_n^2$ is the signal-to-noise ratio and $\text{NL} = \sigma_n^2$ is the noise level.

Power Strength γ . While the original passive detection setting of Bell *et al.* allowed the use of a fixed SNR and NL, this is not the case for our active imaging setting. In active imaging systems, the signal level (and thus the SNR) decreases with distance due to path loss. To compensate for this, a time-varying gain (TVG) gain is applied proportionally to the round-trip distance r_p . This results in the ambient noise level NL being amplified with distance. We thus define a focal point dependent $\gamma(p)$ comprised of

$$\text{NL}(p) [\text{dB}] = \text{DR} - \text{SNR}_0 + G_{\text{TVG}}(r_p) \quad (13)$$

$$\text{SNR}(p) [\text{dB}] = \text{SNR}_0 - \text{PL}(p) \approx \text{SNR}_0 - G_{\text{TVG}}(r_p), \quad (14)$$

where DR is the dynamic range, SNR_0 is the optimal SNR, $\text{PL}(p)$ and $G_{\text{TVG}}(r_p)$ are the path loss and TVG for the focal point p . Note that Eq. (13) assumes that the signal tightly fits the dynamic range while Eq. (14) assumes that the TVG is set similarly to the path loss.

D. Bayesian Inference

Spectral Estimation. Estimating P_s is normally carried out by first substituting the empirical data covariance $\hat{\Sigma}_{\mathbf{x}}$ for the noise covariance $\Sigma_{\mathbf{n}}$ such that $P_s \approx (\mathbf{a}^\dagger \hat{\Sigma}_{\mathbf{x}} \mathbf{a})^{-1}$. For estimating the covariance, as discussed in Section II-II-C, we use subarray averaging [12], where the N -sensor array is divided into K subarrays. This leads to an K -sample estimate of the covariance matrix,

$$\hat{\Sigma}_{\mathbf{x}}(p, c) = \frac{1}{K} \sum_{k=1}^K \mathbf{x}_k(p, c) \mathbf{x}_k^\dagger(p, c). \quad (15)$$

Without subarray averaging, cancellations of coherent signals result in a significant underestimation of the signal power. To avoid this, we use the forward-backward averaged covariance [31, 32, 33] defined as

$$\hat{\Sigma}_{\mathbf{x}, \text{FB}}(p, c) = \frac{1}{2} \left(\hat{\Sigma}_{\mathbf{x}}(p, c) + \mathbf{J} \hat{\Sigma}_{\mathbf{x}}^\top(p, c) \mathbf{J} \right), \quad (16)$$

where \mathbf{J} is the exchange matrix with ones only on the anti-diagonal, and diagonal loading [20]

$$\hat{\Sigma}_{\mathbf{x}, \text{DL}}(p, c) = \hat{\Sigma}_{\mathbf{x}, \text{FB}}(p, c) + \epsilon \text{trace} \left\{ \hat{\Sigma}_{\mathbf{x}, \text{FB}}(p, c) \right\} \mathbf{I} \quad (17)$$

with $\epsilon = 10^{-3}/K$ as recommended by Featherstone [34]. These modifications significantly improve the accuracy of the estimated power [21], which is crucial for our approach.

Prior Distribution. For DoA estimation, it is natural to consider an uninformative prior on the steering angle. Furthermore, using a discrete distribution simplifies the computation associated with performing Bayesian inference. Thus, the previous works [15, 16] have considered setting a uniform discrete prior with a support of $[-\pi, \pi]$ on the steering angle.

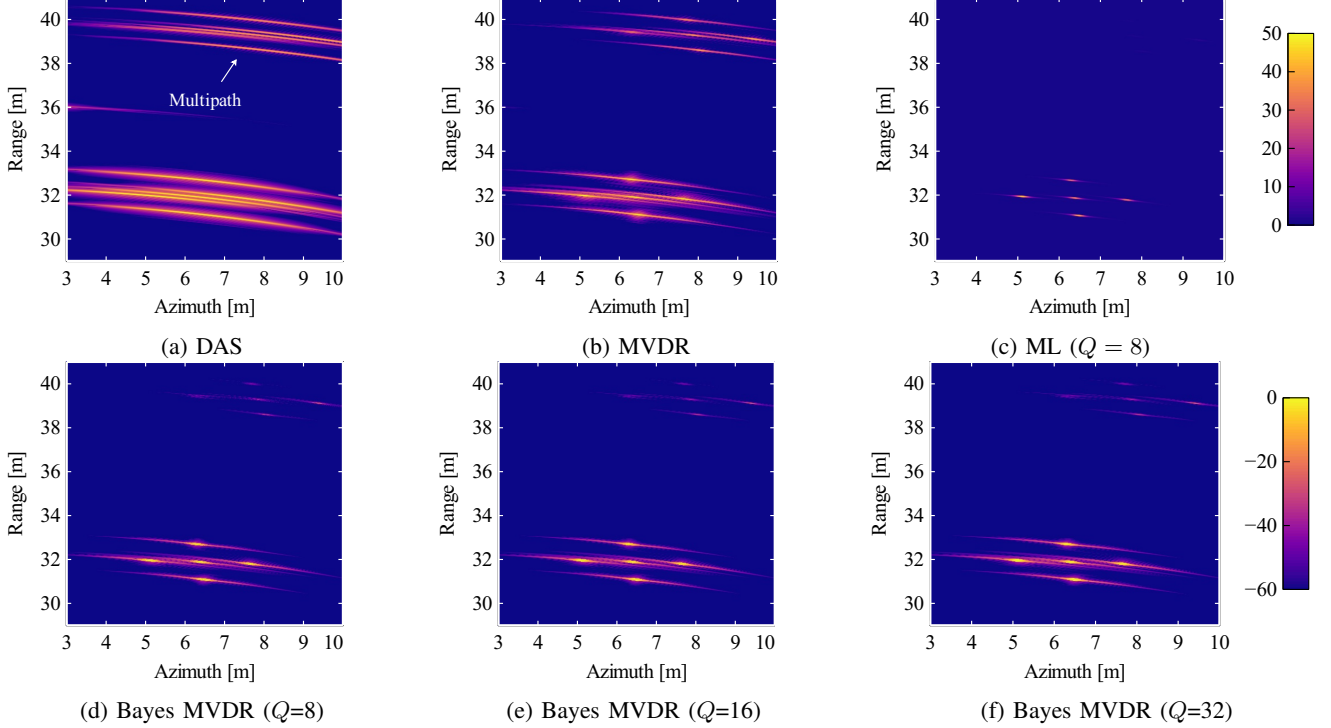


Fig. 1: **Images formed by the methods considered in this work.** The dynamic range of energy-based imaging methods is restricted to 0 dB to 60 dB (color bar in the second row), while the dynamic range of log ML was not restricted and is shown within the range of 0 nats to 50 nats (color bar in the first row). Compared to MVDR, the proposed schemes (Bayes MVDR and ML) achieve lower sidelobes and less pronounced multipath artifacts.

For the speed of sound, we are in a slightly different position: (i) We have an informed guess about the optimal SoS, (ii) but do not know how much the true optimal SoS will deviate from it. Therefore, we consider a continuous informative prior distribution with “soft” boundaries. We choose the prior to follow a normal distribution as $\rho(c) = \mathcal{N}(c; \mu_c, \sigma_c^2)$ with mean μ_c and standard deviation σ_c .

Inference with Gauss-Hermite Quadrature. By choosing a Gaussian prior, we can use Gauss-Hermite quadrature [35]. This provides a principled approach to computing the marginalizing integral (discussed in Section II-II-E) without relying on arbitrary discretization as done in the previous works [15, 16]. Given a computational budget of Q quadrature points, the posterior π is

$$\begin{aligned} \pi_p(c | \mathbf{x}_{1:K}) &= \frac{1}{Z(p)} \tilde{\ell}_p(\mathbf{x}_{1:K} | c) \rho(c) \\ &\propto \tilde{\ell}_p(\mathbf{x}_{1:K} | c) \exp\left(-\frac{1}{2} \frac{(c - \mu_c)^2}{\sigma_c^2}\right) \\ &= \tilde{\ell}_p(\mathbf{x}_{1:K} | \sqrt{2}z\sigma_c + \mu_c) e^{-z^2}, \end{aligned} \quad (18)$$

where we have reparameterized as $c = \sqrt{2}z\mu_c + \sigma_c$ and Z is a normalizing constant, also known as the marginal likelihood or evidence. From this parameterization, the posterior expectation can be computed by setting $e^{-z^2} = u_q$ and $z = z_q$, where for $q = 1, \dots, Q$, z_q is the q th Gauss-Hermite quadrature node, and u_q is the q th Gauss-Hermite weight.

E. Marginalized Adaptive Beamformer

Marginalized Adaptive Beamformer. Given the posterior of c , we compute the marginalized MVDR beamformer as

$$y(p) = \int \mathbf{w}^\dagger(p, c) \mathbf{x}^d(p, c) \pi_p(c | \mathbf{x}_{1:K}) dc \quad (19)$$

$$\approx \frac{1}{\sum_{q=1}^Q v_q} \sum_{q=1}^Q v_q \mathbf{w}^\dagger(p, c) \mathbf{x}^d(p, c), \quad (20)$$

where the unnormalized posterior density is

$$v_q = u_q \ell_p(\mathbf{x}_{1:K} | \sqrt{2}z_q\sigma_c + \mu_c), \quad (21)$$

and $\mathbf{w}(p, c)$ are set as the MVDR fading weights. As mentioned in Section II-II-B, the steering vector is set as $\mathbf{a} = \mathbf{1}$. Also, we reuse the covariance $\widehat{\Sigma}_{\mathbf{x}, \text{DL}}$ used to compute the likelihood in Eq. (21) for finding the MVDR weights in Eq. (3), where the noise covariance estimate is set as $\Sigma = \widehat{\Sigma}_{\mathbf{x}, \text{DL}}$.

Imaging with Marginal Likelihoods. A unique aspect of our Bayesian scheme is that we can obtain the *evidence* of the data. That is, for a pixel p , we can estimate the marginal likelihood

$$Z(p) = \int \tilde{\ell}_p(\mathbf{x}_{1:K} | c) \rho(c) dc \approx \sum_{q=1}^Q v_q. \quad (22)$$

This represents how likely it is to observe the data acquired on p given our model of the system, in particular, the prior. On the flip side, the marginal likelihood can also be interpreted as the evidence for our *model*. If our goal is to detect signals coherent with the Eq. (22) and the prior over the SoS, this

means that we can treat this as the probability of detecting such signal. Therefore, we can use the marginal likelihood in Eq. (22) to image signals. We will refer to this method as “ML” in the experimental section. Also, we will treat the expression in Eq. (22) as the natural scale of this imaging signal, where visualization is done in log scale (“nats”), similarly to other power-based imaging signals.

Computational Cost. The computational cost of computing the marginalized beamformer is proportional to the number of quadrature points Q . More precisely, evaluating a single quadrature point is equivalent to computing a single MVDR beamformer, where the computation linearly increases in Q .

TABLE I: Simulation Settings

Parameter	Val. Unit
Bathymetry depth	100 [m]
Number of sensors	30
Length of array	1 [m]
LFM center freq.	30k [Hz]
LFM bandwidth	20k [Hz]
LFM duration	50 μ [s]
Ambient noise power	80 ^a [dB ^b]
Signal power	190 [dB ^b]
Sampling freq.	500k [Hz]
Sampling duration	0.3 [s]

^a See the text in Section III-III-A.

^b unit: re 1 μ Pa at 1m.

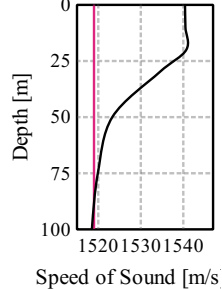


Fig. 2: SoS profile (black). The red line (1519 m/s) is the value used by DAS and MVDR and the mean of our prior on c .

III. EVALUATION

A. Sonar Simulation Setup

Simulation Implementation. We apply our beamformer to active sonar imaging. We simulate point targets with the Bellhop propagation model [18, 19], with an implementation similar to Larsson and Gillard [36], where only a single “ping” is used. The simulation settings are shown in Table I, while the SoS profile is shown in Fig. 2. For the ambient noise, we combine colored noise and white noise, which is more realistic for ocean acoustics [8, Fig. 8.13]. The colored noise follows a power law with exponent 1.4, where the power at 1 Hz is approximately set to be 85 dB re 1 μ Pa at 1m. The white additive Gaussian noise has a power 80 dB re 1 μ Pa at 1m, which represents a relatively high level of ambient noise encountered on a rainy day [8, Fig. 8.13]. The resulting peak SNR is roughly 40 dB. The bathymetry is set to be flat. The array and the linear frequency-modulated (LFM) source are at a depth of 70 m, while the targets are at a depth of 90 m. The beam resolution is evaluated with a single point target at a range of 36 m, while 5 point targets, which are 1 m apart, are arranged as a “cross” for qualitative evaluation.

After simulating propagation, the signal is quantized into 16-bit resolution. Then, we apply a time-varying gain of $G_{TVC}(t) = 20 \log r \approx 20 \log(\pi t c)$ [dB], and demodulate the signal with a quadrature demodulator with a decimation ratio of 4. Range compression is then done by matched filtering.

Baselines and Algorithm Setup. For the baselines, we use the DAS beamformer and the MVDR adaptive beam-

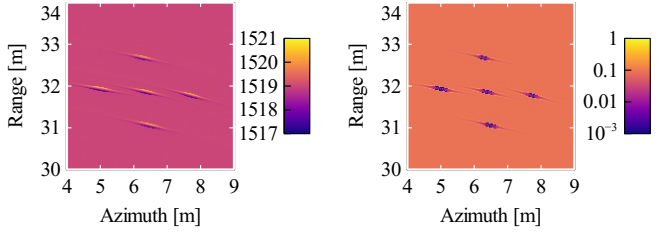


Fig. 3: Posterior estimates of the SoS with $Q = 8$.
TABLE II: Resolution and Multipath Artifact Suppression

	DAS	MVDR	Bayes MVDR	ML
FWHM ¹ [m]	2.27	0.31	0.27	0.08
RPMAL ² [dB]	-9.96	-9.44	-23.99	-42.01

¹ Full width at half maximum

² Relative peak multipath artifact level

former [14]. Both use a constant SoS of 1519 m/s. The DAS beamformer uses Hann fading weights. For the MVDR beamformer, we use subarray averaging, diagonal loading, and forward-backward averaging. We use $K = N/2$ for both the MVDR beamformer and our Bayesian variant (Bayes MVDR). We configure our Bayesian approaches (Bayes MVDR and ML) to use $\text{SNR}_0 = 15$ dB, $\mu_c = 1519$ and $\sigma_c = 0.3$. For the number of quadrature points, $Q \in \{8, 16, 32\}$ is considered. (Note that our method, Bayes MVDR, is the only method that uses numerical quadrature. Therefore, other methods do not involve Q .) Each beamformer outputs a 2-dimensional image of the response across the azimuthal and range direction, which are perpendicular and parallel to the direction the array faces.

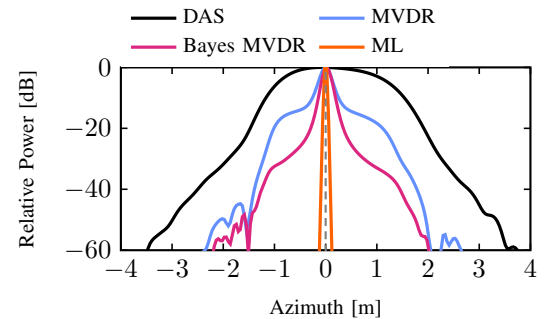


Fig. 4: Normalized azimuth resolution plot for a point target at a range of 30 m. The dotted line shows the azimuth position of the point target.

B. Simulation Results

Qualitative Results. The qualitative results are shown in Fig. 1. The 5-point targets forming a “cross” are near the range of 32 m, while multipath artifacts appear near the range of 39 m. In terms of resolution, our marginalized beamformer (Bayes MVDR) results in lower sidelobes compared to the DAS and MVDR beamformer, resulting in better visibility of the targets. Also, it suppresses the multipath artifacts more effectively compared to the other baselines. Meanwhile, ML imaging performs even better than Bayes MVDR, with the

highest resolution and barely visible multipath artifacts. Note that, for the ML image, we did not restrict the dynamic range whatsoever. Therefore, ML clearly achieves much stronger multipath artifact suppression.

In the second row of Fig. 1, we evaluate the effect of the number of quadrature points, which is directly connected with the computational cost of our method. As shown, the differences between $Q = 8, 16, 32$ are marginal. Quantitatively, the root mean squared error between $Q = 8$ and $Q = 32$ is only -39.13 dB. Therefore, the benefits of our beamformer can be enjoyed with a relatively small number of quadrature points.

To understand the behavior of the marginalized beamformer (Bayes MVDR), we visualize the posterior estimates of the SoS in Fig. 3. In Fig. 3a, we can see that the posterior mean of the SoS deviates from the prior mean near the point targets. Intuitively, the posterior of the SoS is steering the beam towards the direction of the signal. At the same time, the degree of steering is regularized by the uncertainty of the posterior, which can be quantified through the posterior variance shown in Fig. 3b. That is, when the uncertainty is high, the signal is averaged over a wider range of SoS, smoothing out the signal. This smoothing effect is what suppresses the sidelobes and the multipath artifacts.

Quantitative Results. We quantitatively evaluate the resolution and the artifact suppression level. The resolution is measured over a 1-dimensional cutaway along the azimuth axis of one of the point targets, where we normalize the signal level to be in the range of $[0, 1]$ and compute the full width at half-maximum (FWHM) in meters. For the artifact suppression level, we compute the relative peak multipath artifact level (RPMAL), which is the ratio of the peak signal level over the region where the true targets are versus where they are not. For both ML and Bayes MVDR, we used $Q = 8$. The objective metrics are organized in Table II. Bayes MVDR can be seen to achieve better resolution compared to the DAS and MVDR beamformers, where the multipath artifact level is 14dB lower than baselines. Furthermore, ML imaging achieves twice as accurate resolution and close to no artifacts. We visualize the full azimuth resolution plot in Fig. 4.

IV. CONCLUSIONS

In this work, we have presented a Bayesian adaptive beamformer for imaging that marginalizes away the speed of sound. On simulated active sonar data, our beamformer achieved better resolution and improved suppression of multipath artifacts relative to standard DAS and MVDR beamformers. In practice, especially for sonar imaging, it is common to compound the data acquired from multiple “pings” in a synthetic aperture scheme [25, 37]. Combined with this, the resulting images would result in even better resolution. Furthermore, we demonstrated that the marginal likelihood (ML) of the model can be used as a signal for imaging. ML imaging showed promising results and warrants further investigation in the future. Indeed, our method should be applicable to any array-based imaging method, including sonar imaging, medical ultrasound, and seismic imaging: it would be interesting to explore applications in each such context. In the future, evaluating the proposed method on real data

acquired from a moving platform and incorporating various uncertainties in the signal processing chain, not just the speed of sound as we considered here, into a Bayesian model would be worth investigating. Lastly, relaxing the Gaussian noise assumption to other noise distributions could further improve the performance.

REFERENCES

- [1] W. Knight, R. Pridham, and S. Kay, “Digital signal processing for sonar,” *Proc. IEEE*, vol. 69, no. 11, pp. 1451–1506, 1981.
- [2] B. Van Veen and K. Buckley, “Beamforming: A versatile approach to spatial filtering,” *IEEE ASSP Mag.*, vol. 5, no. 2, pp. 4–24, 1988.
- [3] H. L. Van Trees, *Optimum Array Processing*, ser. Detection, Estimation, Modulation Theory. New York, NY: Wiley, 2002, no. 4.
- [4] I. K. Holfort, F. Gran, and J. A. Jensen, “Investigation of sound speed errors in adaptive beamforming,” in *Proceedings of the IEEE Ultrasonics Symposium*, ser. IUS’08. Beijing, China: IEEE, 2008, pp. 1080–1083.
- [5] A. E. A. Blomberg, A. Austeng, R. E. Hansen, and S. A. V. Synnes, “Improving sonar performance in shallow water using adaptive beamforming,” *IEEE J. Oceanic Eng.*, vol. 38, no. 2, pp. 297–307, 2013.
- [6] G. F. Pinton, G. E. Trahey, and J. J. Dahl, “Sources of image degradation in fundamental and harmonic ultrasound imaging using nonlinear, full-wave simulations,” *IEEE Trans. Ultrason., Ferroelect., Freq. Contr.*, vol. 58, no. 4, pp. 754–765, 2011.
- [7] V. Perrot, M. Polichetti, F. Varay, and D. Garcia, “So you think you can DAS? A viewpoint on delay-and-sum beamforming,” *Ultrasonics*, vol. 111, p. 106309, 2021.
- [8] M. A. Ainslie, *Principles of Sonar Performance Modelling*, ser. Springer Praxis Books in Geophysical Sciences. Heidelberg [Germany] London New York Chichester, UK: Springer Published in association with Praxis Pub, 2010.
- [9] P. Stahli, M. Frenz, and M. Jaeger, “Bayesian approach for a robust speed-of-sound reconstruction using pulse-echo ultrasound,” *IEEE Trans. Med. Imaging*, vol. 40, no. 2, pp. 457–467, 2021.
- [10] R. Ali, A. V. Telichko, H. Wang, U. K. Sukumar, J. G. Vilches-Moure, R. Paulmurugan, and J. J. Dahl, “Local sound speed estimation for pulse-echo ultrasound in layered media,” *IEEE Trans. Ultrason., Ferroelect., Freq. Contr.*, vol. 69, no. 2, pp. 500–511, 2022.
- [11] H. Krim and M. Viberg, “Two decades of array signal processing research: The parametric approach,” *IEEE Signal Process. Mag.*, vol. 13, no. 4, pp. 67–94, 1996.
- [12] T.-J. Shan and T. Kailath, “Adaptive beamforming for coherent signals and interference,” *IEEE Trans. Acoust., Speech, Signal Process.*, vol. 33, no. 3, pp. 527–536, 1985.
- [13] K. Bell, Y. Ephraim, and H. Van Trees, “A Bayesian approach to robust adaptive beamforming,” *IEEE Trans. Signal Process.*, vol. 48, no. 2, pp. 386–398, 2000.

[14] O. Frost, "An algorithm for linearly constrained adaptive array processing," *Proc. IEEE*, vol. 60, no. 8, pp. 926–935, 1972.

[15] S. Chakrabarty and E. A. P. Habets, "A Bayesian approach to informed spatial filtering with robustness against DOA estimation errors," *IEEE/ACM Trans. Audio Speech Lang. Process.*, vol. 26, no. 1, pp. 145–160, 2018.

[16] B. A. Yocom, B. R. La Cour, and T. W. Yudichak, "A Bayesian approach to passive sonar detection and tracking in the presence of interferers," *IEEE J. Oceanic Eng.*, vol. 36, no. 3, pp. 386–405, 2011.

[17] C. Lam and A. Singer, "Bayesian beamforming for DOA uncertainty: Theory and implementation," *IEEE Trans. Signal Process.*, vol. 54, no. 11, pp. 4435–4445, 2006.

[18] M. B. Porter and H. P. Bucker, "Gaussian beam tracing for computing ocean acoustic fields," *J. Acoust. Soc. Amer.*, vol. 82, no. 4, pp. 1349–1359, 1987.

[19] H. P. Bucker, "A simple 3-D Gaussian beam sound propagation model for shallow water," *J. Acoust. Soc. Amer.*, vol. 95, no. 5, pp. 2437–2440, 1994.

[20] B. Carlson, "Covariance matrix estimation errors and diagonal loading in adaptive arrays," *IEEE Trans. Aerosp. Electron. Syst.*, vol. 24, no. 4, pp. 397–401, 1988.

[21] B. M. Asl and A. Mahloojifar, "Contrast enhancement and robustness improvement of adaptive ultrasound imaging using forward-backward minimum variance beamforming," *IEEE Trans. Ultrason., Ferroelect., Freq. Contr.*, vol. 58, no. 4, pp. 858–867, 2011.

[22] S. Stergiopoulos, "Implementation of adaptive and synthetic-aperture processing schemes in integrated active-passive sonar systems," *Proc. IEEE*, vol. 86, no. 2, pp. 358–398, 1998.

[23] P. Gerstoft, W. Hodgkiss, W. Kuperman, Heechun Song, M. Siderius, and P. Nielsen, "Adaptive beamforming of a towed array during a turn," *IEEE J. Oceanic Eng.*, vol. 28, no. 1, pp. 44–54, 2003.

[24] A. E. A. Blomberg, "Adaptive beamforming for active sonar imaging," Doctoral Thesis, University of Oslo, 2012.

[25] A. Austeng, A. C. Jensen, C.-I. C. Nilsen, H. J. Callow, and R. E. Hansen, "Use of the minimum variance beamformer in synthetic aperture sonar imaging," in *Proceedings of the European Conference on Underwater Acoustics*, ser. ECUA'12, Edinburgh, Scotland, 2013, p. 070098.

[26] J. I. Buskenes, J. P. Asen, C.-I. C. Nilsen, and A. Austeng, "An optimized GPU implementation of the MVDR beamformer for active sonar imaging," *IEEE J. Oceanic Eng.*, vol. 40, no. 2, pp. 441–451, 2015.

[27] J. I. Buskenes, R. E. Hansen, and A. Austeng, "Low-complexity adaptive sonar imaging," *IEEE J. Oceanic Eng.*, pp. 1–10, 2016.

[28] T. I. Birkenes Lonmo, A. Austeng, and R. E. Hansen, "Improving swath sonar water column imagery and bathymetry with adaptive beamforming," *IEEE J. Oceanic Eng.*, vol. 45, no. 4, pp. 1552–1563, 2020.

[29] J. Capon, "High-resolution frequency-wavenumber spectrum analysis," *Proc. IEEE*, vol. 57, no. 8, pp. 1408–1418, 1969.

[30] A. E. A. Blomberg, C.-I. C. Nilsen, A. Austeng, and R. E. Hansen, "Adaptive sonar imaging using aperture coherence," *IEEE J. Oceanic Eng.*, vol. 38, no. 1, pp. 98–108, 2013.

[31] J. E. Evans, D. F. Sun, and J. R. Johnson, "Application of Advanced Signal Processing Techniques to Angle of Arrival Estimation in ATC Navigation and Surveillance Systems," MIT Lexington Lincoln Lab., Technical Report ADA118306, 1982.

[32] S. Pillai and B. Kwon, "Forward/backward spatial smoothing techniques for coherent signal identification," *IEEE Trans. Acoust., Speech, Signal Process.*, vol. 37, no. 1, pp. 8–15, 1989.

[33] H. Li, J. Li, and P. Stoica, "Performance analysis of forward-backward matched-filterbank spectral estimators," *IEEE Trans. Signal Process.*, vol. 46, no. 7, pp. 1954–1966, 1998.

[34] W. Featherstone, "A novel method to improve the performance of Capon's minimum variance estimator," in *Proceedings of the International Conference on Antennas and Propagation*, vol. 1997. Edinburgh, UK: IEE, 1997, pp. v1–322–v1–322.

[35] F. B. Hildebrand, *Introduction to Numerical Analysis*, ser. Dover Books on Mathematics. Dover Publications, 2003.

[36] A. I. Larsson and C. Gillard, "On waveform selection in a time varying sonar environment," in *Proceedings of ACOUSTICS*. Queensland, Australia: Australian Acoustical Society, 2004, pp. 73–78.

[37] M. P. Hayes and P. T. Gough, "Synthetic aperture sonar: A review of current status," *IEEE J. Oceanic Eng.*, vol. 34, no. 3, pp. 207–224, 2009.